The Electromagnetic Fields of Elliptical Torus Knots

Douglas H. Werner, *Senior Member, IEEE*, D. M. Jones, and P. L. Werner

***Abstract*—The electromagnetic radiation and scattering properties of thin perfectly conducting knotted wires are investigated in this paper. A particular class of knots, which we call elliptical torus knots, are introduced for the purposes of this investigation. These knots derive their name from the fact that they may be constructed on the surface of a virtual torus which has an elliptical cross section. The parameterizations which describe the curves of these knots are more general than any which have been considered in previous studies and, therefore, provide more flexibility in the design of knotted wire scatterers. A moment method technique is applied to model the backscattering from an elliptical trefoil knot as a function of frequency, polarization, and incidence angle.**

***Index Terms*—Electromagnetic radiation and scattering, knot electrodynamics, knotted media, torus knots.**

I. Introduction

THE ELECTROMAGNETIC scattering properties of perfectly conducting thin knotted wires were first studied by Manuar and Jaggard [1]–[3]. The primary objective of this work was to compare the backscatter from a simple knot (the trefoil) to that produced by a simple related unknot (the untrefoil). It was found that a remarkable difference of 25–30 orders of magnitude existed between trefoils and untrefoils in the copolarized backscattering of incident circularly polarized plane waves. This difference in the copolarized backscatter was initially attributed to the topological properties of the knots [2]. However, by considering the backscattering from asymmetric trefoils called morphs, Manuar and Jaggard [4] were able to later demonstrate the dominant role that symmetry plays in producing this effect. This conclusion is supported by the earlier theoretical treatment of the problem where the backscattering from a target with a three-fold or higher order rotation axis has been considered [5]–[7].

The interaction of electromagnetic waves with knotted media, i.e., composite structures with inclusions in the form of simple knots, has been considered in [8]. A simple model for the frequency dispersion of the material parameters associated with knotted media was also suggested in [8]. More recently, a novel technique for designing polarization-selective surfaces (PSSs) using trefoil knot elements was proposed in [9].

The work reported in [10] and [11] represents the first attempt to establish a rigorous mathematical foundation from which analysis techniques may be developed and applied toward the study of knot electrodynamics problems. The analysis methodology presented in [10] and [11] was illustrated by considering a special class of knots, known as (p, q)-torus knots, which have interesting topological as well as electromagnetic properties. It was demonstrated that the well-known trefoil originally studied by Manuar and Jaggard [1]–[4] is one important example of a (p, q)-torus knot. A useful set of parametric representations was developed in [10] and [11] for this particular family of knots by making use of the fact that they may be constructed on the surface of a standard circular torus in $\mathbb{R}^3$. These parameterizations were then used in combination with Maxwell's equations to derive the vector potential and corresponding field expressions which describe the radiation and scattering of electromagnetic waves from circular (p, q)-torus knots. A new electric field integral equation (EFIE) which is well suited for the analysis of thin toroidally knotted wires was also derived in [10] and [11].

The constructions considered in [10] and [11] were restricted to knots which reside on the surface of a torus that has a circular cross section. This paper extends the ideas presented in [10] and [11] by developing a more general set of parameterizations which are valid not only for circular but also for elliptical (p, q)-torus knots. The parametric representations for elliptical (p, q)-torus knots are presented in Section II. It is also demonstrated in Section II how the parameterizations for circular torus knots introduced in [10] and [11] may be obtained as a special case of the more general elliptical torus knot parameterizations. These parameterizations are then used in Section III to derive expressions for the vector potential and electromagnetic fields of elliptical (p, q)-torus knots made from thin perfectly conducting wire. In Section IV, various closed-form expressions are derived for the radiation integrals associated with electrically small elliptical (p, q)-torus knots. Also pointed out in Section IV is the interesting fact that the circular loop as well as the linear dipole geometries can both be obtained as degenerate cases of the elliptical torus knot parameterizations. Finally, some examples illustrating the electromagnetic scattering properties of elliptical trefoils are considered in Section V.

II. Elliptical Torus Knots

In this section, we introduce a useful set of parametric representations for the family of elliptical (p, q)-torus knots. These knots reside on the surface of a torus which has, in general, an elliptical cross section. The geometry for such an elliptical torus is illustrated in Fig. 1. Suppose we let ∂S denote the boundary or surface of the elliptical torus shown in Fig. 1, then the Cartesian coordinates for any point $(x, y, z) \in \partial S$ may be represented by

$$x = (a + b\cos\psi)\cos\varphi \tag{1a}$$

$$y = (a + b\cos\psi)\sin\varphi \tag{1b}$$

$$z = c\sin\psi \tag{1c}$$

where $0 \leq \psi \leq 2\pi$ and $0 \leq \varphi \leq 2\pi$.

Torus knots are classified by the integers p and q which are relatively prime [12], [13]. The numbers p and q tell us how

Manuscript received April 22, 1998; revised December 8, 1999.

The authors are with the Applied Research Laboratory, Pennsylvania State University, State College, PA 16804-0030 USA (e-mail: dhw@psu.edu).

Publisher Item Identifier S 0018-926X(01)03594-3.

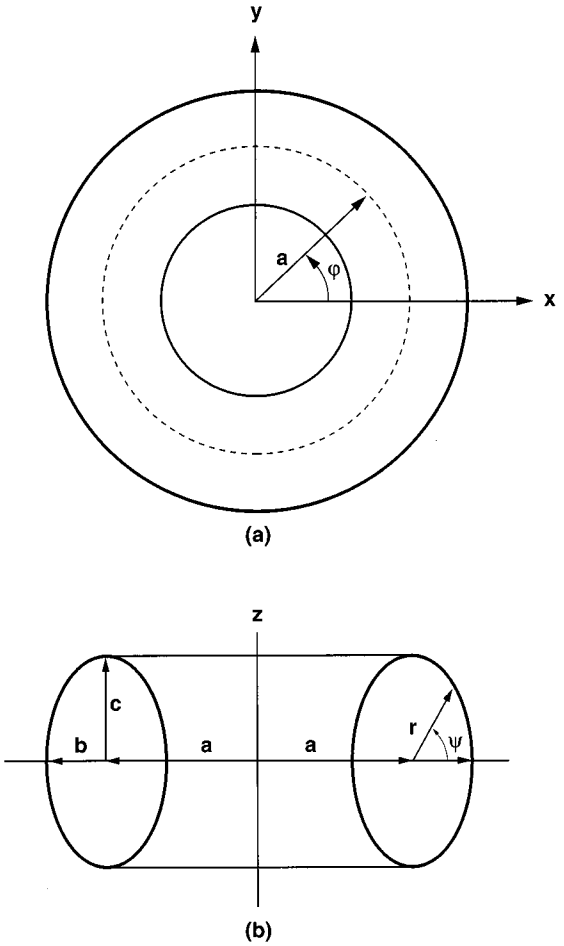

Fig. 1. Geometrical configuration for a torus with an elliptical cross section: (a) the top view and (b) a side view.

many times a particular knot traverses the torus in the longitudinal and meridional directions, respectively. The class of knots which live on the surface of the elliptical torus described by (1a)–(1c) can be shown to have parameterizations given by

$$x = (a + b\cos(\psi + qs))\cos(ps) \tag{2a}$$

$$y = (a + b\cos(\psi + qs))\sin(ps) \tag{2b}$$

$$z = c\sin(\psi + qs) \tag{2c}$$

where $0 \leq s \leq 2\pi$. It is of interest to note here that when $c = b$ the parameterizations for elliptical torus knots given in (2a)–(2c) will reduce to those considered previously in [10] and [11] for circular torus knots. Hence, from a geometrical point of view, circular torus knots may be considered as a special case of the more general elliptical torus knots, even though topologically speaking they are equivalent. This is a subtle yet important distinction since the introduction of an additional degree of freedom through the parameter c allows the electromagnetic characteristics to be studied for a much wider class of knot geometries. Three different geometries for a (2, 3)-torus knot (trefoil) are compared in Fig. 2. These three knotted curves were generated from the parameterizations given in (2a)–(2c) by choosing $c = b/4$, $c = b$, and $c = 4b$. The additional flexibility

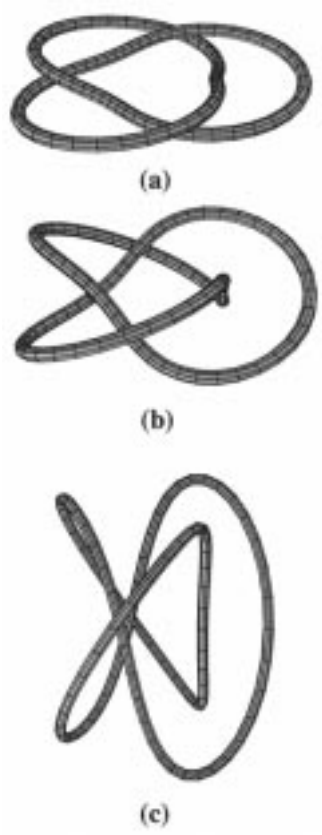

Fig. 2. A comparison of three different trefoil knot geometries generated by choosing (a) $c = b/4$, (b) $c = b$, and (c) $c = 4b$ for a fixed value of a.

provided by elliptical torus knots is also important from a practical point of view. For instance, they offer more control over the resulting electromagnetic properties when used in the design of knotted media and PSS.

III. Electromagnetic Fields

A procedure for deriving electromagnetic field expressions which correspond to knotted wire antennas or scatterers was first introduced in [10], [11]. However, the vector potential and field expressions derived in [11] are restricted to the family of (p, q)-torus knots with circular cross section. In this section, the results reported in [10], [11] are generalized to include knots which reside on the surface of a torus whose cross section is elliptical.

The derivation of these generalized field expressions begins by considering the vector potential representation for an arbitrarily shaped wire with an electric current $\vec{I}$, which is given by [14]

$$\vec{A}(x, y, z) = \frac{\mu}{4\pi}\int_C \vec{I}(x', y', z')\frac{e^{-j\beta R}}{R}\,dl' \tag{3a}$$

where

$$R = \sqrt{(x - x')^2 + (y - y')^2 + (z - z')^2}. \tag{3b}$$

Vector potential expressions for the class of elliptical (p, q)-torus knots may be derived directly from (3a) and (3b) by employing the parameterizations introduced in (2a)–(2c). This approach requires that the knot parameterizations be repre-

sented in terms of the source coordinates as

$$x' = (a + b\cos(\psi + qs'))\cos(ps') \tag{4a}$$

$$y' = (a + b\cos(\psi + qs'))\sin(ps') \tag{4b}$$

$$z' = c\sin(\psi + qs'). \tag{4c}$$

The next step requires finding a suitable expression for the incremental length element dl' which applies to the particular family of elliptical (p, q)-torus knots. This is accomplished by making use of the knot parameterizations given in (4a)–(4c) to obtain (5), shown at the bottom of the page. This suggests that the arclength L of an elliptical torus knot may be obtained directly from (5) by integrating over the curve of the knot. In other words, integrating both sides of (5) over the appropriate limits leads to a useful formula for arclength L_{pq} given by [15]

$$L_{pq} = 2\int_0^{\pi} \sqrt{p^2(a + b\cos u)^2 + q^2(b^2\sin^2 u + c^2\cos^2 u)}\, du. \tag{6}$$

At this stage in the development, we seek to derive a specialized integral representation for the elliptical (p, q)-torus knot vector potential by using (3a) and (3b) in conjunction with (4a)–(4c) and (5). This may be accomplished by following a similar procedure to that outlined in [11]. The resulting expressions for the three components of the vector potential, transformed to spherical coordinates, are given below:

$$\begin{aligned} A_r(r, \theta, \varphi) = {} & \frac{\mu\sin\theta}{4\pi} \cdot \left\{ p\int_0^{2\pi} I_s(s')\,(a + b\cos(\psi + qs')) \right. \\ & \cdot \sin(\varphi - ps') \cdot \frac{e^{-j\beta R}}{R}\, ds' - qb\int_0^{2\pi} I_s(s') \\ & \left. \cdot \sin(\psi + qs')\cos(\varphi - ps')\frac{e^{-j\beta R}}{R}\, ds' \right\} \\ & + \frac{\mu\cos\theta}{4\pi} \left\{ qc\int_0^{2\pi} I_s(s')\cos(\psi + qs') \right. \\ & \left. \cdot \frac{e^{-j\beta R}}{R}\, ds' \right\} \end{aligned} \tag{7a}$$

$$\begin{aligned} A_\theta(r, \theta, \varphi) = {} & \frac{\mu\cos\theta}{4\pi} \left\{ p\int_0^{2\pi} I_s(s')\,(a + b\cos(\psi + qs')) \right. \\ & \cdot \sin(\varphi - ps')\frac{e^{-j\beta R}}{R}\, ds' - qb\int_0^{2\pi} I_s(s') \\ & \left. \cdot \sin(\psi + qs')\cos(\varphi - ps')\frac{e^{-j\beta R}}{R}\, ds' \right\} \\ & - \frac{\mu\sin\theta}{4\pi} \left\{ qc\int_0^{2\pi} I_s(s')\cos(\psi + qs') \right. \\ & \left. \cdot \frac{e^{-j\beta R}}{R}\, ds' \right\} \end{aligned} \tag{7b}$$

$$\begin{aligned} A_\varphi(r, \theta, \varphi) = {} & \frac{\mu}{4\pi} \cdot \left\{ p\int_0^{2\pi} I_s(s')\,(a + b\cos(\psi + qs')) \right. \\ & \cdot \cos(\varphi - ps')\frac{e^{-j\beta R}}{R}\, ds' + qb\int_0^{2\pi} I_s(s') \\ & \left. \cdot \sin(\psi + qs')\sin(\varphi - ps')\frac{e^{-j\beta R}}{R}\, ds' \right\} \end{aligned} \tag{7c}$$

where $I_s(s')$ represents the current distribution on the surface of the knotted wire. These expressions for the vector potential are valid everywhere, including in the near-zone of the knots. However, the approximation

$$\frac{e^{-j\beta R}}{R} \approx \frac{e^{-j\beta r}}{r}\,\Gamma(s') \tag{8a}$$

where

$$\Gamma(s') = e^{j\beta[(a + b\cos(\psi + qs'))\cos(\varphi - ps')\sin\theta + c\sin(\psi + qs')\cos\theta]} \tag{8b}$$

$$r = \sqrt{x^2 + y^2 + z^2} \tag{8c}$$

may be used to find simplified far-zone vector potential representations. In particular, by substituting (8a) into (7b) and (7c) we obtain the following far-zone approximations for A_θ and A_φ:

$$\begin{aligned} A_\theta(r, \theta, \varphi) \approx {} & \frac{\mu\cos\theta}{4\pi}\,\frac{e^{-j\beta r}}{r} \cdot \left\{ p\int_0^{2\pi} I_s(s')\,(a + b\cos(\psi + qs')) \right. \\ & \cdot \sin(\varphi - ps')\Gamma(s')\, ds' - qb\int_0^{2\pi} I_s(s') \\ & \left. \cdot \sin(\psi + qs')\cos(\varphi - ps')\Gamma(s')\, ds' \right\} \\ & - \frac{\mu\sin\theta}{4\pi}\,\frac{e^{-j\beta r}}{r} \left\{ qc\int_0^{2\pi} I_s(s')\cos(\psi + qs') \right. \\ & \left. \cdot \Gamma(s')\, ds' \right\} \end{aligned} \tag{9a}$$

$$\begin{aligned} A_\varphi(r, \theta, \varphi) \approx {} & \frac{\mu}{4\pi}\,\frac{e^{-j\beta r}}{r} \cdot \left\{ p\int_0^{2\pi} I_s(s')\,(a + b\cos(\psi + qs')) \right. \\ & \cdot \cos(\varphi - ps')\Gamma(s')\, ds' + qb\int_0^{2\pi} I_s(s') \\ & \left. \cdot \sin(\psi + qs')\sin(\varphi - ps')\Gamma(s')\, ds' \right\}. \end{aligned} \tag{9b}$$

Finally, far-zone expressions for the electromagnetic fields produced by elliptical torus knots may be obtained directly from (9a) and (9b) by making use of the following well-known rela-

$$dl' = \sqrt{p^2(a + b\cos(\psi + qs'))^2 + q^2(b^2\sin^2(\psi + qs') + c^2\cos^2(\psi + qs'))}\, ds'. \tag{5}$$

tionships [14]:

$$E_r \approx 0 \tag{10a}$$

$$E_\theta \approx -j\omega A_\theta \tag{10b}$$

$$E_\varphi \approx -j\omega A_\varphi \tag{10c}$$

$$H_r \approx 0 \tag{10d}$$

$$H_\theta \approx j\frac{\omega}{\eta} A_\varphi = -\frac{E_\varphi}{\eta} \tag{10e}$$

$$H_\varphi \approx -j\frac{\omega}{\eta} A_\theta = \frac{E_\theta}{\eta}. \tag{10f}$$

There are several potentially useful applications of the general electromagnetic field expressions for elliptical torus knots given in (9a)–(9b) and (10a)–(10f) above. For instance, the scattering matrix of the elliptical torus could be easily obtained from these field representations. The scattering matrix is defined by

$$\begin{pmatrix} E_{hs} \\ E_{vs} \end{pmatrix} = \frac{e^{-j\beta r}}{r} \begin{pmatrix} S_1 & S_2 \\ S_3 & S_4 \end{pmatrix} \begin{pmatrix} E_{hi} \\ E_{vi} \end{pmatrix} \tag{11}$$

where the elements can be found from the geometric and material properties of the scattering medium [16]. This type of analysis could be useful for characterizing the anisotropy corresponding to a particular torus knot by investigating the properties of the matrix elements S_2 and S_3. A similar type of approach could be followed in order to determine the related Stokes parameters [16].

IV. Special Cases

A. Circular Torus Knots

The first special case that will be considered involves knots which are formed by winding a piece of wire around the surface of a virtual circular torus. The circular torus knots can be thought of as resulting from a degenerate form of the elliptical torus knots, namely, when $c = b$. In this case, the expressions for the vector potential given in (7a)–(7c) reduce to

$$\begin{aligned} A_r(r, \theta, \varphi) = {} & \frac{\mu \sin\theta}{4\pi} \\ & \cdot \left\{ p \int_0^{2\pi} I_s(s')\,(a + b\cos(\psi + qs')) \right. \\ & \quad \cdot \sin(\varphi - ps')\frac{e^{-j\beta R}}{R}\,ds' - qb \int_0^{2\pi} I_s(s') \\ & \quad \left. \cdot \sin(\psi + qs')\cos(\varphi - ps')\frac{e^{-j\beta R}}{R}\,ds' \right\} \\ & + \frac{\mu\cos\theta}{4\pi} \left\{ qb \int_0^{2\pi} I_s(s')\cos(\psi + qs') \right. \\ & \quad \left. \cdot \frac{e^{-j\beta R}}{R}\,ds' \right\} \end{aligned} \tag{12a}$$

$$\begin{aligned} A_\theta(r, \theta, \phi) = {} & \frac{\mu\cos\theta}{4\pi} \\ & \cdot \left\{ p \int_0^{2\pi} I_s(s')\,(a + b\cos(\psi + qs')) \right. \\ & \quad \cdot \sin(\varphi - ps')\frac{e^{-j\beta R}}{R}\,ds' - qb \int_0^{2\pi} I_s(s') \\ & \quad \left. \cdot \sin(\psi + qs')\cos(\varphi - ps')\frac{e^{-j\beta R}}{R}\,ds' \right\} \\ & - \frac{\mu\sin\theta}{4\pi} \left\{ qb \int_0^{2\pi} I_s(s')\cos(\psi + qs') \right. \\ & \quad \left. \cdot \frac{e^{-j\beta R}}{R}\,ds' \right\} \end{aligned} \tag{12b}$$

$$\begin{aligned} A_\varphi(r, \theta, \varphi) = {} & \frac{\mu}{4\pi} \\ & \cdot \left\{ p \int_0^{2\pi} I_s(s')\,(a + b\cos(\psi + qs')) \right. \\ & \quad \cdot \cos(\varphi - ps')\frac{e^{-j\beta R}}{R}\,ds' + qb \int_0^{2\pi} I_s(s') \\ & \quad \left. \cdot \sin(\psi + qs')\sin(\varphi - ps')\frac{e^{-j\beta R}}{R}\,ds' \right\} \end{aligned} \tag{12c}$$

which are in agreement with the results reported in [11]. Likewise, approximate far-zone expressions for the vector potential components associated with circular torus knots may be obtained by setting $c = b$ in (9a) and (9b).

B. Small-Knot Approximation (b and c are Functions of a)

Suppose we assume that b and c are proportional to a such that $b = \alpha a$ and $c = \gamma a$ where $0 \le \alpha \le 1/2$. In this case, (8b) and (8c) may be written as

$$\Gamma(s') = e^{j\beta a[(1+\alpha\cos(\psi+qs'))\cos(\varphi-ps')\sin\theta + \gamma\sin(\psi+qs')\cos\theta]}. \tag{13}$$

When a is small enough, (13) can be approximated by

$$\begin{aligned} \Gamma(s') \approx {} & 1 + j\beta a\,(1 + \alpha\cos(\psi + qs'))\cos(\varphi - ps')\sin\theta \\ & + j\beta a\gamma\sin(\psi + qs')\cos\theta. \end{aligned} \tag{14}$$

Another approximation which may be made in the case of electrically small torus knots is that the current distribution on these knots will be uniform. Therefore, by setting $I_s(s') = I_0$ where I_0 is a constant, the far-zone vector potential expressions given in (9a) and (9b) may be reduced to the form

$$\begin{aligned} A_\theta(r, \theta, \varphi) = {} & \frac{\mu a I_0 \cos\theta}{4\pi}\,\frac{e^{-j\beta r}}{r} \\ & \cdot \left\{ p \int_0^{2\pi} (1 + \alpha\cos(\psi + qs')) \right. \\ & \quad \cdot \sin(\varphi - ps')\Gamma(s')\,ds' - q\alpha \\ & \quad \left. \cdot \int_0^{2\pi} \sin(\psi + qs')\cos(\varphi - ps')\Gamma(s')\,ds' \right\} \\ & - \frac{\mu a I_0 \sin\theta}{4\pi}\,\frac{e^{-j\beta r}}{r} \\ & \cdot \left\{ q\gamma \int_0^{2\pi} \cos(\psi + qs')\Gamma(s')\,ds' \right\} \end{aligned} \tag{15a}$$

$$A_\varphi(r,\theta,\varphi)=\frac{\mu a I_0}{4\pi}\frac{e^{-j\beta r}}{r}\cdot\left\{p\int_0^{2\pi}(1+\alpha\cos(\psi+qs'))\cdot\cos(\varphi-ps')\Gamma(s')\,ds'+q\alpha\int_0^{2\pi}\cdot\sin(\psi+qs')\sin(\varphi-ps')\Gamma(s')\,ds'\right\} \tag{15b}$$

Finally, simple closed-form representations for the fields produced by electrically small torus knots may be found by substituting (14) into (15a) and (15b) and evaluating the required integrals.

The general far-zone expressions presented in this section are valid for all values of p and q, with the exception of the two special cases when $p = q$ and $p = 2q$. For this reason, the general expressions given below hold for most cases of practical interest. It can be shown that the general form of the small-knot far-zone vector potential is

$$A_\theta \approx 0 \tag{16a}$$

$$A_\varphi \approx j\frac{\mu\beta I_0\sin\theta}{4}\,p\left[a^2+\frac{b^2}{2}\right]\frac{e^{-j\beta r}}{r}. \tag{16b}$$

Using (10a)–(10f), the far-field representations for these small knots can then be determined to be

$$E_r \approx 0 \tag{17a}$$

$$E_\theta \approx 0 \tag{17b}$$

$$E_\varphi \approx \frac{\eta\beta^2 I_0\sin\theta}{4}\,p\left[a^2+\frac{b^2}{2}\right]\frac{e^{-j\beta r}}{r} \tag{17c}$$

$$H_r \approx 0 \tag{17d}$$

$$H_\theta \approx -\frac{\beta^2 I_0\sin\theta}{4}\,p\left[a^2+\frac{b^2}{2}\right]\frac{e^{-j\beta r}}{r} \tag{17e}$$

$$H_\varphi \approx 0. \tag{17f}$$

We note here the fact that the far-zone representations given in (17a)–(17f) are independent of γ or c. Hence, under these conditions, the far-zone expressions for the elliptical torus knots are the same as those derived for the circular torus knots in [11]. It was shown in [11] that (17a)–(17f) are equivalent to the far field that would be produced by an electrically small loop with an effective radius r_e and number of turns N given by

$$r_e=\sqrt{a^2+\frac{b^2}{2}} \tag{18a}$$

$$N = p. \tag{18b}$$

C. Small-Knot Approximation (c is Independent of a and b)

The next special case that will be considered is that in which the horizontal radii a and b of the torus are small in comparison to the vertical radius c. In this instance, we let b be proportional to a such that $b = \alpha a$ where $0 \le \alpha \le 1/2$. We also make the assumption that c is independent of both a and b. Hence, for sufficiently small values of a, the following approximation for (8b) and (8c) can be justified:

$$\Gamma(s') \approx [1+j\beta a(1+\alpha\cos(\psi+qs'))\cos(\varphi-ps')\sin\theta]\cdot e^{j\beta c\sin(\psi+qs')\cos\theta}. \tag{19}$$

Substituting (19) into (15a) and (15b) and evaluating the required integrals leads to convenient closed-form expressions for A_θ and A_φ. The resulting expressions for the general case as well as a special case of interest are summarized in the following two sections.

1) General Case ($p/q \neq 2n$, $p/q \neq 2n-1$ and $p/q \neq (2n-1)/2$): The general expressions for the far-zone vector potential and fields presented in this section are valid for the majority of possible torus knot configurations. It can be shown that the general form of the far-zone vector potential components A_θ and A_φ are

$$A_\theta \approx 0 \tag{20a}$$

$$A_\varphi \approx j\frac{\mu I_0}{4}\frac{e^{-j\beta r}}{r}\,p\beta a^2\sin\theta\cdot\left\{J_0(x)+\frac{\alpha^2}{2}[J_0(x)+J_2(x)]\right\} \tag{20b}$$

$$\text{where } x=\beta c\cos\theta. \tag{20c}$$

These expressions hold provided $p/q \neq 2n$, $p/q \neq 2n-1$, and $p/q \neq (2n-1)/2$ where $n \in \mathbb{N}$. Far-zone representations for the electromagnetic fields in the general case may be obtained directly from (20a) and (20b) by making use of (10a)–(10f). The resulting far-field expressions are

$$E_r \approx 0 \tag{21a}$$

$$E_\theta \approx 0 \tag{21b}$$

$$E_\varphi \approx \frac{\eta\beta^2 I_0}{4}\frac{e^{-j\beta r}}{r}\,pa^2\sin\theta\cdot\left\{J_0(x)+\frac{\alpha^2}{2}\,[J_0(x)+J_2(x)]\right\} \tag{21c}$$

$$H_r \approx 0 \tag{21d}$$

$$H_\theta \approx -\frac{\beta^2 I_0}{4}\frac{e^{-j\beta r}}{r}\,pa^2\sin\theta\cdot\left\{J_0(x)+\frac{\alpha^2}{2}\,[J_0(x)+J_2(x)]\right\} \tag{21e}$$

$$H_\varphi \approx 0. \tag{21f}$$

2) Special Case When $p/q = (2n-1)/2$: The closed-form expressions for the vector potential in this case where $p/q = (2n-1)/2$ and $n \in \mathbb{N}$ are given by

$$A_\theta \approx j\frac{\mu I_0}{4}\frac{e^{-j\beta r}}{r}\,\beta a^2\frac{\alpha}{2}\,\sin\theta\cos\theta\sin\left(2\varphi+\frac{2p}{q}\,\psi\right)\cdot\left[(2p+q)J_{(2p+q)/q}(x)+(2p-q)J_{(2p-q)/q}(x)\right] \tag{22a}$$

Fig. 3. The geometry for a trefoil formed by a (3, 2)-torus knot.

$$A_\varphi \approx j\frac{\mu I_0}{4}\frac{e^{-j\beta r}}{r}\beta a^2\sin\theta \cdot\left\{p\left[J_0(x)+\frac{\alpha^2}{2}\left(J_0(x)+J_2(x)\right)\right] +\cos\left(2\varphi+\frac{2p}{q}\psi\right)\cdot\left[p\alpha\left(J_{(2p+q)/q}(x)+J_{(2p-q)/q}(x)\right) + q\frac{\alpha}{2}\left(J_{(2p+q)/q}(x)-J_{(2p-q)/q}(x)\right)\right]\right\} \quad (22b)$$

and the corresponding far-field representations are

$$E_r \approx 0 \quad (23a)$$

$$E_\theta \approx \frac{\eta\beta^2 I_0}{4}\frac{e^{-j\beta r}}{r}a^2\frac{\alpha}{2}\sin\theta\cos\theta\sin\left(2\varphi+\frac{2p}{q}\psi\right)\cdot\left[(2p+q)J_{(2p+q)/q}(x)+(2p-q)J_{(2p-q)/q}(x)\right] \quad (23b)$$

$$E_\varphi \approx \frac{\eta\beta^2 I_0}{4}\frac{e^{-j\beta r}}{r}a^2\sin\theta \cdot\left\{p\left[J_0(x)+\frac{\alpha^2}{2}\left(J_0(x)+J_2(x)\right)\right] +\cos\left(2\varphi+\frac{2p}{q}\psi\right)\cdot\left[p\alpha\left(J_{(2p+q)/q}(x)+J_{(2p-q)/q}(x)\right) + q\frac{\alpha}{2}\left(J_{(2p+q)/q}(x)-J_{(2p-q)/q}(x)\right)\right]\right\} \quad (23c)$$

$$H_r \approx 0 \quad (23d)$$

$$H_\theta \approx -\frac{\beta^2 I_0}{4}\frac{e^{-j\beta r}}{r}a^2\sin\theta \cdot\left\{p\left[J_0(x)+\frac{\alpha^2}{2}\left(J_0(x)+J_2(x)\right)\right] +\cos\left(2\varphi\frac{2p}{q}\psi\right)\cdot\left[p\alpha\left(J_{(2p+q)/q}(x)+J_{(2p-q)/q}(x)\right) + q\frac{\alpha}{2}\left(J_{(2p+q)/q}(x)-J_{(2p-q)/q}(x)\right)\right]\right\} \quad (23e)$$

$$H_\varphi \approx \frac{\beta^2 I_0}{4}\frac{e^{-j\beta r}}{r}a^2\frac{\alpha}{2}\sin\theta\cos\theta\sin\left(2\varphi+\frac{2p}{q}\psi\right)\cdot\left[(2p+q)J_{(2p+q)/q}(x)+(2p-q)J_{(2p-q)/q}(x)\right]. \quad (23f)$$

The geometry for the special case in which $p=3$ and $q=2$ (i.e., $p/q=3/2$) is illustrated in Fig. 3. It can easily be seen that the (3, 2)-torus knot shown in Fig. 3 is a trefoil. We make the observation here that even though the (2, 3)-torus knot and the (3, 2)-torus knot are topologically equivalent, they do not produce the same radiated or scattered fields. This can be seen by comparing (21a)–(21f) with $p=2$ to (23a)–(23f) with $p=3$ and $q=2$.

D. Circular Loop and Linear Dipole

1) Circular Loop: For the special case when $b=c=0$ and $p=1$, the torus knot parameterizations defined in (2a)–(2c) describe a circular loop of radius a. Hence, the general vector potential expressions for the (p, q)-torus knots derived in (7a)–(7c) will reduce to the well-known classical results for the circular loop antenna given by [17]

$$A_r = \frac{\mu a\sin\theta}{4\pi}\int_0^{2\pi} I_s(\varphi')\sin(\varphi-\varphi')\frac{e^{-j\beta R}}{R}\,d\varphi' \quad (24a)$$

$$A_\theta = \frac{\mu a\cos\theta}{4\pi}\int_0^{2\pi} I_s(\varphi')\sin(\varphi-\varphi')\frac{e^{-j\beta R}}{R}\,d\varphi' \quad (24b)$$

$$A_\varphi = \frac{\mu a}{4\pi}\int_0^{2\pi} I_s(\varphi')\cos(\varphi-\varphi')\frac{e^{-j\beta R}}{R}\,d\varphi' \quad (24c)$$

where

$$R=\sqrt{r^2+a^2-2ar\sin\theta\cos(\varphi-\varphi')}. \quad (24d)$$

2) Linear Dipole: In addition to the circular loop, the linear dipole can also be obtained as a degenerate case of the elliptical torus knot parameterizations. To demonstrate this, suppose we let $a=b=0$, then the expressions for the vector potential components given in (7a)–(7c) reduce to

$$A_r = \frac{\mu\cos\theta}{4\pi}qc\int_0^{2\pi} I_s(s')\cos(\psi+qs')\frac{e^{-j\beta R}}{R}\,ds' \quad (25a)$$

$$A_\theta = -\frac{\mu\sin\theta}{4\pi}qc\int_0^{2\pi} I_s(s')\cos(\psi+qs')\frac{e^{-j\beta R}}{R}\,ds' \quad (25b)$$

$$A_\varphi = 0. \quad (25c)$$

By making the change of variables

$$z' = c\sin(\psi+qs') \quad (26a)$$

$$dz' = qc\cos(\psi+qs')\,ds' \quad (26b)$$

with $q=1/2$ and $\psi=-\pi/2$, (25a) and (25b) may be written as

$$A_r = \frac{\mu\cos\theta}{4\pi}\int_{-c}^{c} I_s(z')\frac{e^{-j\beta R}}{R}\,dz' \quad (27a)$$

$$A_\theta = -\frac{\mu\sin\theta}{4\pi}\int_{-c}^{c} I_s(z')\frac{e^{-j\beta R}}{R}\,dz'. \quad (27b)$$

Fig. 4. Top and side views of an elliptical (2, 3)-torus knot (i.e., a trefoil).

Transforming from spherical coordinates to cylindrical coordinates yields

$$A_z = \frac{\mu}{4\pi} \int_{-c}^{c} I_s(z') \frac{e^{-j\beta R}}{R}\, dz' \tag{28a}$$

where

$$R = \sqrt{(z - z')^2 + \rho^2} \tag{28b}$$

$$\rho = \sqrt{x^2 + y^2}. \tag{28c}$$

This is the well-known classical result for the vector potential of a z-directed linear dipole of length $2c$ [14].

V. Results

Fig. 4 shows a top and side view of an elliptical trefoil knot. Top and side views of a piecewise-linear thin-wire model of this trefoil have also been included for visualization purposes in Fig. 5. The trefoil is assumed to be constructed from perfectly conducting wire with an arclength of 41.416 mm and a radius of 5.528×10^{-2} mm. The parameters which describe this knot were chosen such that $p = 2$, $q = 3$, $\alpha = 1/4$, and $\gamma = 4$.

A procedure for calculating the scattering cross section of thin knotted wires was outlined in [11]. This procedure makes use of the well-known equation for scattering cross section given by

$$\sigma = 4\pi r^2 \frac{\left|\vec{E}^s\right|^2}{\left|\vec{E}^i\right|^2} \tag{29}$$

where $\vec{E}^i$ and $\vec{E}^s$ represent the incident and scattered electric fields, respectively. Suppose we consider the trefoil knot shown in Figs. 4 and 5. A linearly polarized plane wave with an intensity of 1 V/m is assumed to be incident on the knot. The corresponding scattering field is determined using a rigorous numerical analysis procedure based on the method of moments. The piecewire linear segmentation used to construct the method of moments model of the elliptical trefoil knot is clearly visible

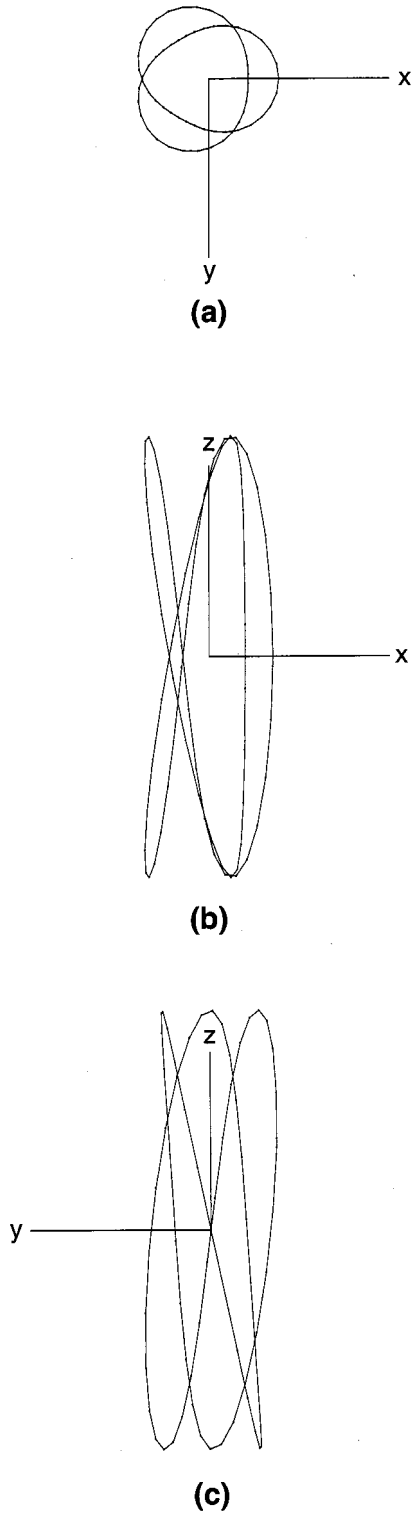

Fig. 5. Top and side views of a thin-wire method of moments model for the elliptical trefoil shown in Fig. 4.

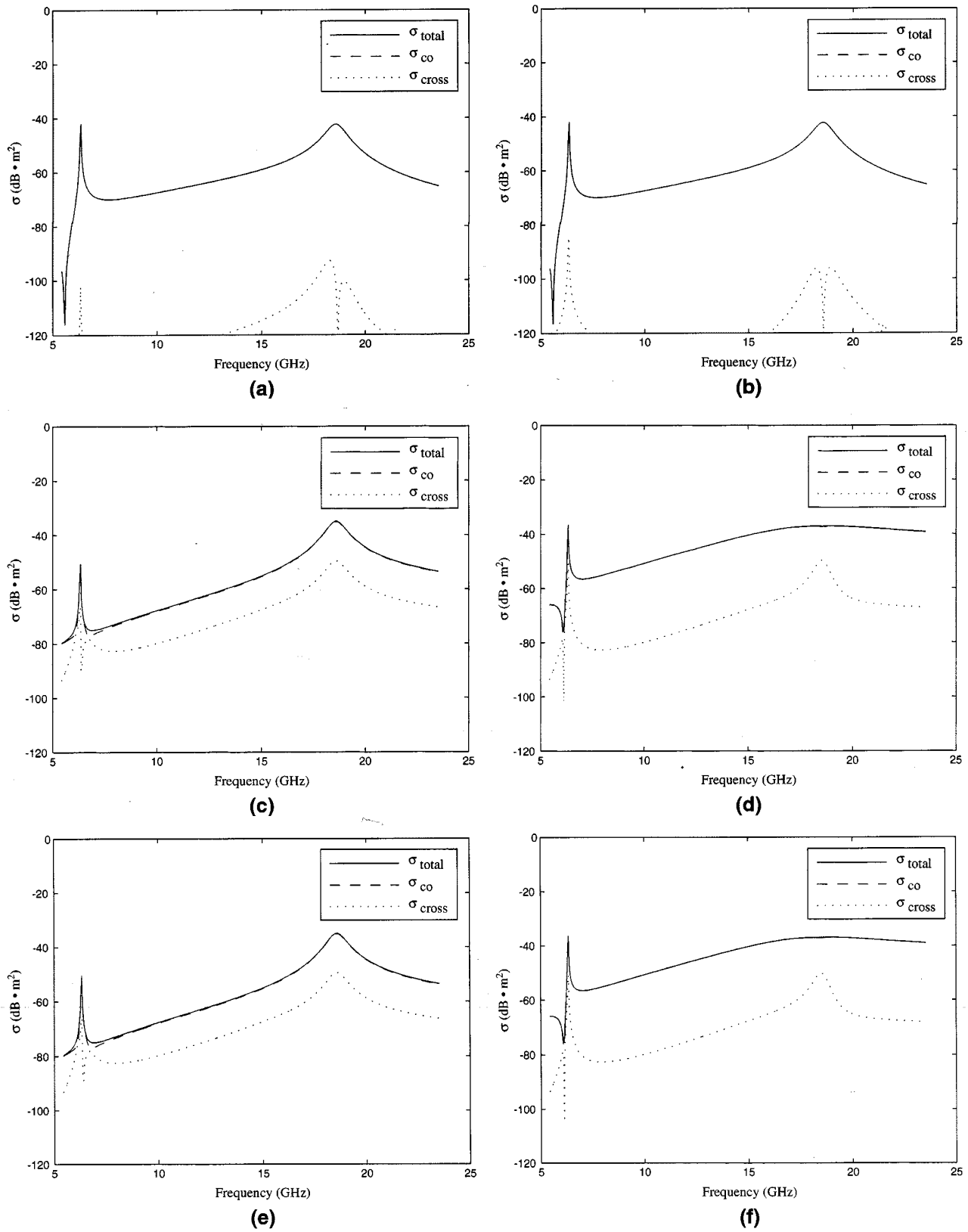

Fig. 6. Backscatter cross section versus frequency for the elliptical (2, 3)-torus knot illustrated in Figs. 4 and 5. A linearly polarized plane wave is assumed to be incident on the knot traveling in the (a) positive z direction with the electric field parallel to the x-axis, (b) positive z direction with the electric field parallel to the y-axis, (c) positive y direction with the electric field parallel to the x-axis, (d) positive y direction with the electric field parallel to the z-axis, (e) positive x direction with the electric field parallel to the y-axis, and (f) positive x direction with the electric field parallel to the z-axis.

in Fig. 5. Fig. 6 contains several plots which illustrate how the backscatter cross section of this knot depends on frequency, polarization, and angle of incidence. An inspection of the plots shown in Fig. 6 reinforces earlier observations made in [11]

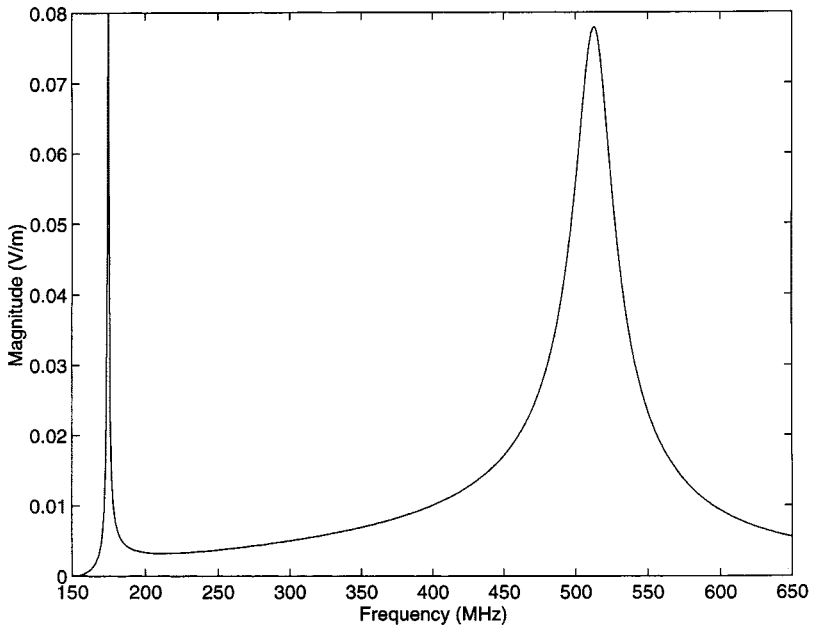

Fig. 7. Magnitude of the backscattered field in V/m versus frequency for an elliptical (2, 3)-torus knot with an arclength of 1.5 m. A linearly polarized plan wave is assumed to be incident on the knot traveling in the positive z direction with the electric field parallel to the x- or y-axis.

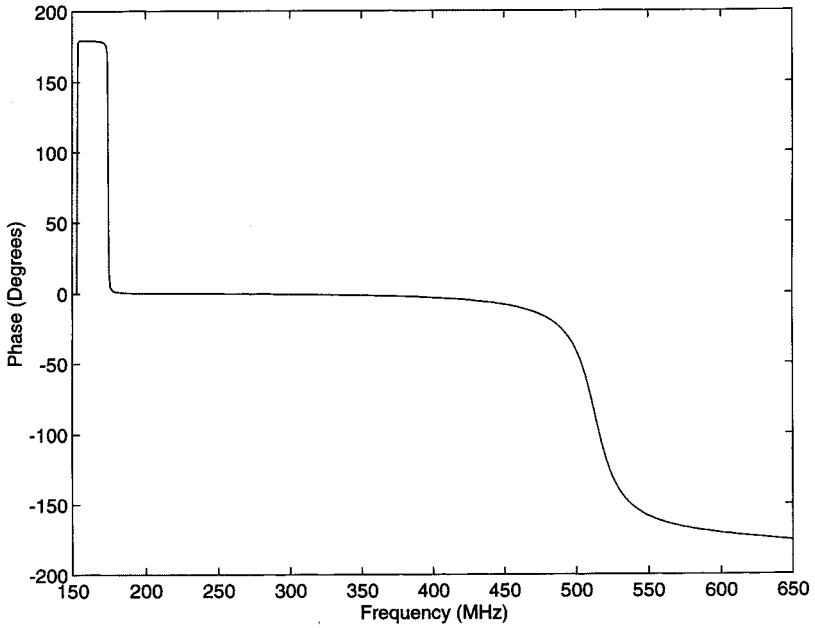

Fig. 8. Relative phase of the backscattered field in degrees versus frequency for an elliptical (2, 3)-torus knot with an arclength of 1.5 m. A linearly polarized plane wave is assumed to be incident on the knot traveling in the positive z direction with the electric field parallel to the x- or y-axis.

which suggested that trefoil knots experience a strong field coupling for all possible polarizations and angles of incidence.

We next compare the on-axis backscattering characteristics of an elliptical (2, 3)-torus knot with those of a circular (2, 3)-torus knot that has an equivalent arc length of 1.5 m. Figs. 7 and 8 show the magnitude and phase, respectively, of the scattered field as a function of frequency produced by the elliptical trefoil. On the other hand, Figs. 9 and 10 show the same set of plots for the corresponding circular trefoil. An inspection of these plots reveals a particularly interesting feature in the phase response that is characteristic of the scattered field produced by (2, 3)-torus knots. Namely, there exists a region above the first resonance where the phase of the backscattered field with respect to the incident field is very close to zero degrees. This is particularly true of the elliptical (2, 3)-torus knot, where the relative phase remains close to zero degrees over a fairly wide bandwidth, ranging from about 175 MHz to at least 475 MHz (see Fig. 8). This suggests that elliptical torus knots with this property may also have application to the synthesis of broadband artificial magnetic media [18], [19].

One of the most important advantages of elliptical torus knots is that their geometry can be controlled in such a way that they

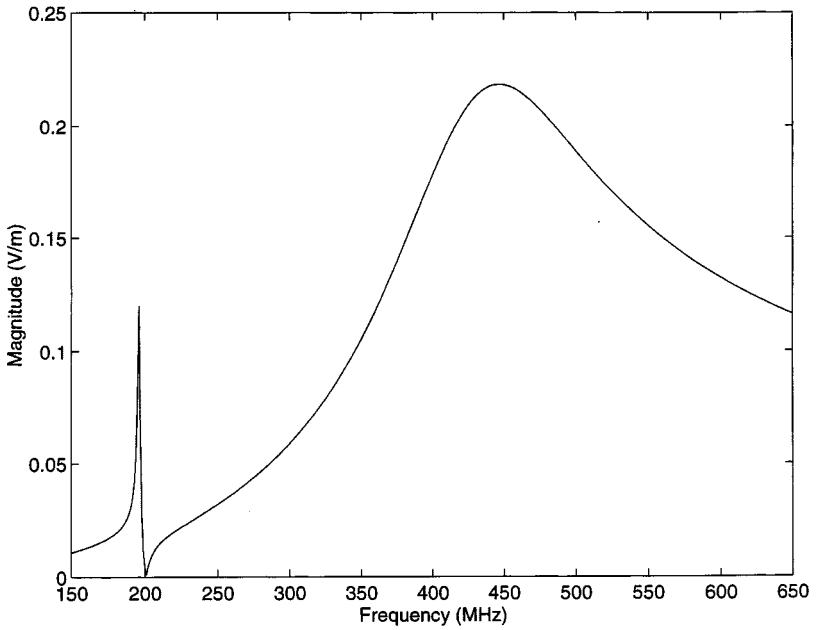

Fig. 9. Magnitude of the backscattered field in V/m versus frequency for a circular (2, 3)-torus knot with an arclength of 1.5 m. A linearly polarized plane wave is assumed to be incident on the knot traveling in the positive z direction with the electric field parallel to the x- or y-axis.

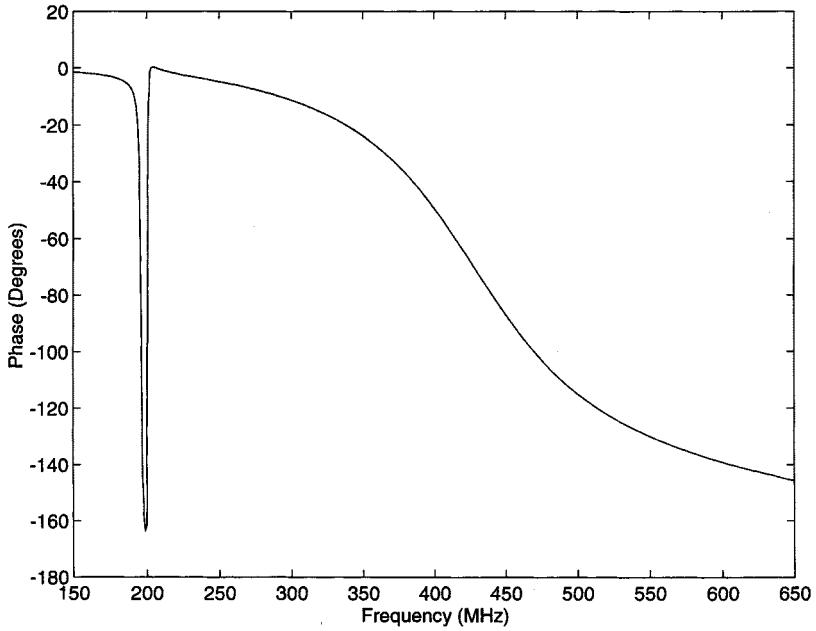

Fig. 10. Relative phase of the backscattered field in degrees versus frequency for a circular (2, 3)-torus knot with an arclength of 1.5 m. A linearly polarized plane wave is assumed to be incident on the knot traveling in the positive z direction with the electric field parallel to the x- or y- axis.

behave more like a loop in one extreme and more like a dipole in the other extreme. Hence, depending upon the application, a proper balance between the loop and dipole characteristics of a particular elliptical torus knot presumably could be found. This kind of flexibility is not possible with the circular torus knots considered in [11], which can be made to have radiation and scattering characteristics close to a loop, but not a dipole.

Finally, we note that up to this point we have primarily focused on how the scattering from torus knots is affected by their geometrical structure. However, it may also be of interest to consider the relationship between the topology of the knots and the corresponding scattered fields. One approach for doing this has been suggested in [20], where structures based on toroidal links are introduced for the purpose of emphasizing topological relationships over geometrical ones.

VI. Conclusion

A useful set of parameterizations were introduced in this paper for elliptical (p, q)-torus knots. This family of knots

derive their name from the fact that they reside on the surface of a torus which has an elliptical cross section. These parameterizations allow more flexibility in controlling the shape of the knots when compared with those previously considered in [10] and [11]. In fact, this paper demonstrates that the parameterizations for circular torus knots originally introduced in [10] and [11] are actually a special case of the more general elliptical torus knot parameterizations. Near-zone as well as far-zone expressions were derived for the vector potential and electromagnetic fields produced by elliptical (p, q)-torus knots comprised of thin perfectly conducting wire. Several convenient closed-form expressions were found for the far fields of electrically small elliptical torus knots. It was also shown that the circular loop as well as the linear dipole geometries may both be obtained as degenerate forms of the parametric representations for elliptical torus knots. Finally, a rigorous numerical modeling technique based on the method of moments was used to evaluate the scattering properties of several elliptical torus knots.

APPENDIX

In this appendix, a methodology is presented for evaluating integrals of the type

$$I(v, x) = \int_{u_1}^{u_2} \cos(vu + x \sin u)\, du \tag{30}$$

where

$$v = \frac{n}{q},\ n \in \mathbb{I} \quad \text{and} \quad q \in \mathbb{N} \tag{31}$$

$$x = \beta c \cos\theta \tag{32}$$

$$u_1 = 0 \tag{33}$$

$$u_2 = 2\pi q. \tag{34}$$

These integrals are encountered in the process of deriving the far-zone representations for the vector potential components A_θ and A_φ considered in Section IV-C. The first step toward finding a closed-form solution to (30) is to recognize that since v and x are real valued quantities (i.e., $v, x \in \mathbb{R}$), we may write

$$I(v, x) = \Re\left\{\int_{u_1}^{u_2} e^{j[vu + x \sin u]}\, du\right\}. \tag{35}$$

Next, we make use of the generating function for Bessel functions [21]

$$e^{x(t-1/t)/2} = \sum_{k=-\infty}^{\infty} J_k(x) t^k, \qquad t \neq 0. \tag{36}$$

Setting $t = e^{ju}$ in (36) gives

$$e^{jx \sin u} = \sum_{k=-\infty}^{\infty} J_k(x) e^{jku}. \tag{37}$$

Multiplying both sides of (37) by e^{jvu} and integrating with respect to u leads to

$$\int_{u_1}^{u_2} e^{j[vu + x \sin u]}\, du = \sum_{k=-\infty}^{\infty} J_k(x) \int_{u_1}^{u_2} e^{j(v+k)u}\, du. \tag{38}$$

From (35) and (38), it follows that

$$\begin{aligned} I(v, x) &= \Re\left\{\sum_{k=-\infty}^{\infty} J_k(x) \int_{u_1}^{u_2} e^{j(v+k)u}\, du\right\} \\ &= \sum_{k=-\infty}^{\infty} J_k(x) \Re\left\{\int_{u_1}^{u_2} e^{j(v+k)u}\, du\right\} \\ &= \sum_{k=-\infty}^{\infty} J_k(x) \int_{u_1}^{u_2} \cos\left[(v+k)u\right] du \\ &= \sum_{k=-\infty}^{\infty} J_k(x) \left[\frac{\sin\left[(v+k)u_2\right] - \sin\left[(v+k)u_1\right]}{v+k}\right]. \end{aligned} \tag{39}$$

Finally, by substituting the appropriate values of $u_1 = 0$ and $u_2 = 2\pi q$ into (39), we arrive at

$$I(v, x) = \begin{cases} 2\pi q J_{-v}(x), & v \in \mathbb{I} \\ 0, & v \notin \mathbb{I}. \end{cases} \tag{40}$$

A closed-form solution to the related integrals

$$I(v, -x) = \int_{u_1}^{u_2} \cos(vu - x \sin u)\, du \tag{41}$$

may be obtained directly from (40) as

$$I(v, -x) = \begin{cases} 2\pi q J_v(x), & v \in \mathbb{I} \\ 0, & v \notin \mathbb{I}. \end{cases} \tag{42}$$

REFERENCES

[1] O. Manuar and D. L. Jaggard, "Backscatter signature of knots," *Opt. Lett.*, vol. 20, pp. 115–117, Jan. 1995.

[2] D. L. Jaggard and O. Manuar, "Can one 'hear' the handedness or topology of a knot," in *Proc. IEEE Antennas and Propagation Society Int. Symp. URSI Radio Science Meeting*, Newport Beach, CA, June 1995, URSI Digest, p. 244.

[3] O. Manuar and D. L. Jaggard, "Wave interactions with trefoils and untrefoils," in *Proc. IEEE Antennas and Propagation Society Int. Symp. and URSI Radio Science Meeting*, Baltimore, MD, July 1996, URSI Digest, p. 279.

[4] ——, "Scattering from knots and unknots: The role of symmetry," *Electron. Lett.*, vol. 33, no. 4, pp. 278–280, Feb. 1997.

[5] C. E. Baum and H. N. Kritikos, Eds., *Electromagnetic Symmetry*. Washington, DC: Taylor and Francis, 1995, pp. 19–21.

[6] C. E. Baum, "SEM backscattering,", Interaction Note 476, 1989.

[7] ——, "SEM and EEM scattering matrices, and time-domain scatterer polarization in the scattering residue matrix," in *Direct and Inverse Methods in Radar Polarimetry*, W. M. Boerner, Ed. Novwell, MA: D. Riedel, 1992, pp. 427–486.

[8] S. A. Tretyakov, A. A. Sochava, and S. I. Maslovski, "Plane wave propagation in a class of knotted media," *Electromagnetics*, vol. 16, pp. 203–212, 1996.
[9] J. V. Hagen, D. H. Werner, and R. Mittra, "Polarization selective surfaces composed of trefoil knot elements," *Microw. Opt. Technol. Lett.*, vol. 21, no. 3, pp. 170–173, May 1999.
[10] D. H. Werner, "The electrodynamics of torus knots," in *IEEE Antennas and Propagation Society Int. Symp. Dig.*, vol. 2, Montreal, Canada, July 1997, pp. 1468–1471.
[11] ——, "Radiation and scattering from thin toroidally knotted wires," *IEEE Trans. Antennas Propagat.*, vol. 47, pp. 1351–1363, Aug. 1999.
[12] C. C. Adams, *The Knot Book: An Elementary Introduction to the Mathematical Theory of Knots*. New York: W. H. Freeman and Company, 1994.
[13] H. Seifert and W. Threlfall, *A Textbook of Topology*. New York: Academic, 1980.
[14] C. A. Balanis, *Antenna Theory, Analysis and Design*. New York: Wiley, 1982.
[15] D. H. Werner, "Electromagnetic radiation and scattering from elliptical torus knots," in *IEEE Antennas and Propagation Soc. Int. Symp. Dig.*, vol. 1, Atlanta, GA, July 1998, pp. 858–861.
[16] L. Tsang, J. A. Kong, and R. T. Shin, *Theory of Microwave Remote Sensing*. New York: Wiley, 1985, sec. 3.2.
[17] D. H. Werner, "An exact integration procedure for vector potentials of thin circular loop antennas," *IEEE Trans. Antennas Propagat.*, vol. 44, pp. 157–165, Feb. 1996.
[18] J. V. Hagen, P. Werner, R. Mittra, and D. H. Werner, "Toward the synthesis of an artificial magnetic medium," in *Proc. IEEE Antennas and Propagation Society Int. Symp.*, vol. 1, Orlando, FL, July 1999, pp. 430–433.
[19] J. V. Hagen, R. Mittra, P. L. Werner, and D. H. Werner, "Toward the synthesis of artificial magnetic media," *IEEE Microwave Guided Wave Lett.*, vol. 27, no. 1, pp. 27–30, 2000.
[20] O. Manuar and D. L. Jaggard, "Topology in scattering," *Electron. Lett.*, vol. 34, no. 25, pp. 2426–2428, Dec. 1998.
[21] L. C. Andrews, *Special Functions for Engineers and Applied Mathematicians*. New York: MacMillan, 1985.

Douglas H. Werner (S'81–M'89–SM'94) joined the Faculty of the Pennsylvania State University Department of Electrical Engineering as an Associate Professor in July of 1998. He is a member of the Communications and Space Sciences Lab (CSSL) and is affiliated with the Electromagnetics Communication Research Lab. He also has a joint appointment as a Senior Research Associate with the Electromagnetics and Environmental Effects Department of the Applied Research Laboratory at Penn State, where he has worked since 1990. His research interests include theoretical and computational electromagnetics with applications to antenna theory and design, microwaves, wireless and personal communication systems, electromagnetic wave interactions with complex materials, fractal and knot electrodynamics, and genetic algorithms. He has published numerous technical papers and proceedings articles and is the author of six book chapters. He recently published a new book for IEEE Press entitled *Frontiers in Electromagnetics*. He has also contributed a chapter for a Wiley Interscience book entitled *Electromagnetic Optimization by Genetic Algorithms* and has been invited to prepare a monograph on *Fractal Antennas*.

Dr. Werner received the 1993 Applied Computational Electromagnetics Society (ACES) Best Paper Award. He was also the recipient of a 1993 URSI International Young Scientist Award. In 1994, he received the Pennsylvania State University Applied Research Laboratory Outstanding Publication Award. In March 2000 he was the recipient of a College of Engineering PSES Outstanding Research Award. He was also recently presented with an IEEE Central Pennsylvania Section Millennium Medal. He is an Associate Editor of *Radio Science* and a member of the American Geophysical Union (AGU), URSI Commissions B and G, the Applied Computational Electromagnetics Society (ACES), Eta Kappa Nu, Tau Beta Pi, and Sigma Xi.

D. M. Jones, photograph and biography not available at the time of publication.

P. L. Werner, photograph and biography not available at the time of publication.